Langmuir
Article
pubs.acs.org/Langmuir

The Complex Thiol−Palladium Interface: A Theoretical and Experimental Study

Pilar Carro,*[,†] Gastón Corthey,[‡] Aldo A. Rubert,[‡] Guillermo A. Benitez,[‡] Mariano H. Fonticelli,[‡] and Roberto C. Salvarezza[‡]

[†]*Departamento de Química Física, Universidad de La Laguna, Tenerife, Spain, and* [‡]*Instituto de Investigaciones Fisicoquímicas Teóricas y Aplicadas (INIFTA), Universidad Nacional de La Plata - CONICET, Sucursal 4 Casilla de Correo 16, (1900) La Plata, Argentina*

Received June 20, 2010. Revised Manuscript Received August 11, 2010

This paper presents a theoretical study of the surface structures and thermodynamic stability of different thiol and sulfide structures present on the palladium surface as a function of the chemical potential of the thiol species. It has been found that as the chemical potential of the thiol is increased, the initially clean palladium surface is covered by a $(\sqrt{3} \times \sqrt{3})$R30° sulfur lattice. Further increase in the thiol pressure or concentration leads to the formation of a denser $(\sqrt{7} \times \sqrt{7})$R19.1° sulfur lattice, which finally undergoes a phase transition to form a complex $(\sqrt{7} \times \sqrt{7})$R19.1° sulfur + thiol adlayer (3/7 sulfur + 2/7 thiol coverage). This transition is accompanied by a strong reconstruction of the Pd(111) surface. The formation of these surface structures has been explained in terms of the catalytic properties of the palladium surface. These results have been compared with X-ray photoelectron spectroscopy results obtained for thiols adsorbed on different palladium surfaces.

1. Introduction

Self-assembled monolayers (SAMs) of alkanethiols on metals have attracted considerable attention because of the possibility to control the physical chemistry of surfaces at the molecular level.[1] This control has made possible several innovative applications ranging from molecular electronics to catalysis.[1,2]

The self-assembly of alkanethiols on Pd(111) surfaces (2D) is particularly interesting because the organic/metal interface formed involves a mixed layer containing both sulfides and thiols,[3] much more complex than the thiol/Au(111) interface.[4] The palladium/sulfide interface, which has been proposed on the basis of X-ray photoelectron spectroscopy (XPS) measurements,[3] enhances the SAM stability against wet-chemical etchants compared with the alkanethiolate SAMs on gold.[5] Nevertheless, whereas the state of the art regarding the structure of thiols on Au(111) is actually advanced,[6−14] the structure of the thiol/Pd(111) interface is farther from being completely understood, and only a few works on this topic have been published.[3,15]

On the other hand, thiols are usually employed as a capping for palladium nanoparticles.[16] However, the structure of the thiol/palladium interface in these particles is still not clear. Although a massive sulfidization of the nanoparticles appears to be possible,[17−20] a disulfide SAM structure on octanethiol-protected palladium nanoparticles has also been proposed.[21] Nevertheless, the sulfidization model seems to fit better with the results observed in the case of bulk palladium surfaces. In both cases, planar and nanoparticle surfaces, the sulfur atoms could be formed due to S−C bond scission during the alkanethiol self-assembly or cluster growth, respectively.

Elucidation of the surface structure of alkanethiols adsorbed on palladium is difficult because even the adsorption of sulfur on palladium is rather complex. It has been shown that during exposure of the Pd(111) surface to H_2S at 300 K, a $(\sqrt{3} \times \sqrt{3})$R30° S overlayer is initially formed.[22] Increasing the annealing to 400 K results in the formation of a $(\sqrt{7} \times \sqrt{7})$R19° S lattice. Subsequent annealing of the $(\sqrt{3} \times \sqrt{3})$R30° structure at 700 K causes it to convert into a $(\sqrt{7} \times \sqrt{7})$R19° overlayer without evidence of sulfur atoms at the surface. In the latter case, the lack of activity toward dissociative hydrogen adsorption suggests that

*Corresponding author (e-mail pcarro@ull.es).

(1) Love, J.; Estroff, L.; Kriebel, J.; Nuzzo, R.; Whitesides, G. *Chem. Rev.* **2005**, *105*, 1103–1170.
(2) Gates, B. D.; Xu, Q.; Stewart, M.; Ryan, D.; Willson, C. G.; Whitesides, G. M. *Chem. Rev.* **2005**, *105*, 1171–1196.
(3) Love, J.; Wolfe, D.; Haasch, R.; Chabinyc, M.; Paul, K.; Whitesides, G.; Nuzzo, R. *J. Am. Chem. Soc.* **2003**, *125*, 2597–2609.
(4) Vericat, C.; Vela, M. E.; Salvarezza, R. C. *Phys. Chem. Chem. Phys.* **2005**, *7*, 3258–3268.
(5) Love, J.; Wolfe, D.; Chabinyc, M.; Paul, K.; Whitesides, G. *J. Am. Chem. Soc.* **2002**, *124*, 1576–1577.
(6) Jadzinsky, P. D.; Calero, G.; Ackerson, C. J.; Bushnell, D. A.; Kornberg, R. D. *Science* **2007**, *318*, 430–433.
(7) Walter, M.; Akola, J.; Lopez-Acevedo, O.; Jadzinsky, P. D.; Calero, G.; Ackerson, C. J.; Whetten, R. L.; Grönbeck, H.; Häkkinen, H. *Proc. Natl. Acad. Sci. U. S. A.* **2008**, *105*, 9157–9162.
(8) Cossaro, A.; Mazzarello, R.; Rousseau, R.; Casalis, L.; Verdini, A.; Kohlmeyer, A.; Floreano, L.; Scandolo, S.; Morgante, A.; Klein, M. L.; Scoles, G. *Science* **2008**, *321*, 943–946.
(9) Rzeźnicka, I. I.; Lee, J.; Maksymovych, P.; Yates, J. T. *J. Phys. Chem. B* **2005**, *109*, 15992–15996.
(10) Maksymovych, P.; Sorescu, D. C.; Yates, J. T. *Phys. Rev. Lett.* **2006**, *97*, 146103.
(11) Grönbeck, H.; Häkkinen, H. *J. Phys. Chem. B* **2007**, *111*, 3325–3327.
(12) Häkkinen, H.; Walter, M.; Grönbeck, H. *J. Phys. Chem. B* **2006**, *110*, 9927–9931.
(13) Jiang, D.; Dai, S. *J. Phys. Chem. C* **2009**, *113*, 7838–7842.
(14) Grönbeck, H.; Häkkinen, H.; Whetten, R. L. *J. Phys. Chem. C* **2008**, *112*, 15940–15942.
(15) Majumder, C. *Langmuir* **2008**, *24*, 10838–10842.
(16) Zamborini, F.; Gross, S.; Murray, R. *Langmuir* **2001**, *17*, 481–488.
(17) Murayama, H.; Ichikuni, N.; Negishi, Y.; Nagata, T.; Tsukuda, T. *Chem. Phys. Lett.* **2003**, *376*, 26–32.
(18) Sun, Y.; Frenkel, A. I.; Isseroff, R.; Shonbrun, C.; Forman, M.; Shin, K.; Koga, T.; White, H.; Zhang, L.; Zhu, Y.; Rafailovich, M. H.; Sokolov, J. C. *Langmuir* **2006**, *22*, 807–816.
(19) Ramallo-López, J.; Giovanetti, L.; Craievich, A.; Vicentin, F.; Marín-Almazo, M.; José-Yacaman, M.; Requejo, F. *Phys. B* **2007**, *389*, 150–154.
(20) Yang, Z.; Klabunde, K. J.; Sorensen, C. M. *J. Phys. Chem. C* **2007**, *111*, 18143–18147.
(21) Zelakiewicz, B. S.; Lica, G. C.; Deacon, M. L.; Tong, Y. *J. Am. Chem. Soc.* **2004**, *126*, 10053–10058.
(22) Miller, J. B.; Gellman, A. J. *Surf. Sci.* **2009**, *603*, L82–L85.

sulfur exerts its influence on surface chemistry from subsurface locations. Therefore, understanding of the thiol/palladium system should also involve the study of the sulfur/palladium surface structure.

Recently we have found, by using electrochemical techniques and XPS, that the adlayer formed by alkanethiol adsorption on palladium consists of thiolates and sulfides with coverages of $\theta_{sulfide} \approx 0.4$ and $\theta_{thiolate} \approx 0.3$.[23] The value $\theta_{thiolate} \approx 0.3$ is close to that found for thiolate SAMs on gold, where they form a $(\sqrt{3} \times \sqrt{3})$R30° and its c(4 × 2) superlattice ($\theta_{thiolate} = 0.33$).[4] This complex layer explains the barrier properties found in the electrochemical measurements. The value $\theta_{sulfide} \approx 0.4$ is consistent with the formation of diluted palladium sulfide layers such as $(\sqrt{7} \times \sqrt{7})$R19.1° with $\theta_{sulfide} = 0.43$, a previously reported lattice.[24]

The complex nature of this interface explains why, even today, many studies of thiol self-assembly on palladium surfaces ignore or avoid discussing experimental and theoretical results in light of the thiol−S−Pd surface structure.[15,25] Therefore, a study on the reactivity of palladium upon thiol adsorption, the formation of the different surface structures, and their stability under different experimental conditions is needed to understand the self-assembly of thiols on palladium surfaces.

In this work, we have made a theoretical study of surface structures of the methanethiol radical (SCH_3, MT) and sulfur (S) that can be present on the palladium surface and their stability analysis as a function of the chemical potential of thiol in the gas phase. Although there are many possible surface structures for this complex system, we have restricted our study to those surface structures with S coverage near 0.4 ML ($\theta_{sulfide} \approx 0.4$), the value experimentally observed for thiols on palladium.[23] Moreover, the sulfide lattices considered were the ones described by experimental and theoretical studies for sulfur adsorption on palladium.[24,26−28] On the other hand, we have limited our analysis of thiolate surface structures on the Pd and S/Pd surfaces to those that exhibit a nearly complete thiolate monolayer consistent with the experimentally observed $\theta_{thiolate} \approx 0.3$ and the barrier properties of the adlayer.[23]

We have found that, as the chemical potential of the thiol is increased, the initially clean palladium surface can be covered by a $(\sqrt{3} \times \sqrt{3})$R30° S lattice. Further increase in the pressure or concentration leads to the formation of $(\sqrt{7} \times \sqrt{7})$R19.1° S, which then undergoes a transition to form a complex $(\sqrt{7} \times \sqrt{7})$R19.1° (S + MT) adlayer. This transition is accompanied by a strong surface reconstruction of the Pd(111) surface. The formation of these surface structures has been explained in terms of the catalytic properties of the palladium surface, and the theoretical results have been compared with XPS results obtained for thiols adsorbed on different palladium surfaces.

2. Computational Details

In this work we have carried out a thermodynamic stability study of the methanethiol radical (MT) and sulfur (S) layers on Pd(111), using density functional theory (DFT). The calculations were performed using the VASP code (version 4.6).[29,30] The surfaces were modeled as slabs of periodic material in two dimensions and containing five metallic layers. The three outermost atomic metal layers as well as the atomic coordinates of MT were allowed to relax without further constraints. The repeated slabs were separated from each other by a vacuum space of ∼10 Å. The total energy and optimized geometry for all of the structures were obtained using the Perdew−Wang (PW91) implementation of the generalized gradient approach for the exchange correlation (*xc*) potential.[31] The one-electron wave functions were expanded on a plane wave basis set with a cutoff of 420 eV for the kinetic energy. The Brillouin zone sampling was done according to the Monkhorst−Pack[32] scheme with a 5 × 5 × 1 mesh of special *k* points for the $(\sqrt{7} \times \sqrt{7})$R19.1° unit cell and 9 × 9 × 1 mesh for the $(\sqrt{3} \times \sqrt{3})$R30° one. The projector augmented wave (PAW) method[33] was employed to describe the effect of the inner cores of the atoms on the valence electrons. The tolerance used to define self-consistency was 10^{-5} eV for the single-point total energy and 10^{-4} eV for the geometry optimization. The energy minimization (electronic density relaxation) for a given nuclear configuration was carried out using a Davidson−Bloch iteration scheme. The dipole correction was applied to minimize polarization effects caused by asymmetry of the slabs.

We have carried out a convergence test regarding the cutoff energy for the plane waves as well as the *k* point grid for our systems, the difference in electronic energy being < 0.1 eV. Therefore, the error in surface free energy is about 3 meV/Å^2.

The energy minimization (electronic density relaxation) for a given nuclear configuration was carried out using a Davidson−Bloch iteration scheme. The dipole correction was applied to minimize polarization effects caused by asymmetry of the slabs.

The calculated lattice constant for bulk Pd was found to be 3.96 Å, which is within ∼2% of the experimental value. To accomplish the different proposed models for adsorption on this metallic surface, we have used two different surface unit cells on the Pd(111) surface: $(\sqrt{3} \times \sqrt{3})$R30° and $(\sqrt{7} \times \sqrt{7})$R19.1°.

We have determined the stability of different MT/S adsorbed surface structures on Pd(111) compared with respect to the clean metal by using the surface free energy at finite temperature and pressure in the framework of the first-principles atomistic thermodynamics,[34] following our previous results for thiols on gold.[35−37] We have taken into account that the adsorbed thiols can be fragmented on the Pd(111) surface, leading to adsorbed S as determined by XPS measurements. Thus, the surface free energy can be written as

$$\gamma(T,p) = \frac{1}{A}[G_{total} - N_{Pd}g_{Pd} - N_S\mu_S - N_{MT}\mu_{MT}] - \gamma_{clean} \quad (1)$$

where A is the surface area, G_{total} is the Gibbs free energy of the adsorbed system, and g_{Pd}, μ_S, and μ_{MT} are the chemical potentials of the bulk metal surface and the adsorbates, S and MT, respectively. N_{Pd}, N_S, and N_{MT} are the number of Pd atoms and the adsorbed species in the slab unit cell. On the other hand, γ_{clean} represents the surface free energy of the clean surface.

In eq 1 the chemical potential of the Pd surface (g_{Pd}) is equated to the total energy of a bulk Pd atom (E^{Pd}_{bulk}). On the other hand, the Gibbs free energy (G_{total}) is estimated by the total energy of the adsorbate−substrate system at $T = 0$ K (E_{total}). We define the surface free energy of the clean Pd surface as

$$\gamma_{clean} = \frac{1}{A}[E^{Pd} - N_{Pd}E^{Pd}_{bulk}] - \gamma^{U}_{clean} \quad (2)$$

(23) Corthey, G.; Rubert, A. A.; Benitez, G. A.; Fonticelli, M. H.; Salvarezza, R. C. *J. Phys. Chem. C* **2009**, *113*, 6735–6742.
(24) Alfonso, D. R. *Surf. Sci.* **2005**, *596*, 229–241.
(25) Pomfret, M. B.; Pietron, J. J.; Owrutsky, J. C. *Langmuir* **2010**, *26*, 6809–6817.
(26) Liu, W.; Mitchell, K. A. R.; Berndt, W. *Surf. Sci.* **1997**, *393*, L119–L125.
(27) Alfonso, D. R. *Surf. Sci.* **2007**, *601*, 4899–4909.
(28) Alfonso, D. R. *Surf. Sci.* **2006**, *600*, 4508–4516.
(29) Kresse, G.; Joubert, D. *Phys. Rev. B* **1999**, *59*, 1758.
(30) Kresse, G.; Furthmüller, J. *Phys. Rev. B* **1996**, *54*, 11169.
(31) Perdew, J. P.; Wang, Y. *Phys. Rev. B* **1992**, *45*, 13244.
(32) Kresse, G.; Hafner, J. *Phys. Rev. B* **1993**, *47*, 558.
(33) Blöchl, P. E. *Phys. Rev. B* **1994**, *50*, 17953.
(34) Reuter, K.; Scheffler, M. *Phys. Rev. B* **2001**, *65*, 035406.
(35) Torres, D.; Carro, P.; Salvarezza, R. C.; Illas, F. *Phys. Rev. Lett.* **2006**, *97*, 226103–4.
(36) Carro, P.; Salvarezza, R.; Torres, D.; Illas, F. *J. Phys. Chem. C* **2008**, *112*, 19121–19124.
(37) Carro, P.; Creus, A. H.; Muñoz, A.; Salvarezza, R. C. *Langmuir* **2010**, *26*, 9589–9595.

where γ^{U}_{clean} is the surface free energy of the unreconstructed Pd(111) surface, which has to be subtracted because the slab model exhibits two surfaces, one without adsorbate and another one with the adsorbate, and E^{Pd} is the total energy of the clean surface slab.

The chemical potential of the $(CH_3S)_2$ molecule is related to those of MT and S by the following equation:

$$\frac{\mu_{(CH_3S)_2}}{2} = \mu_{MT} = \mu_S + \mu_C + \frac{3}{2}\mu_{H_2} \quad (3)$$

The species involved in eq 3 have been reported in previous studies of similar reactions on Pd surfaces. In fact, it has been shown that methane decomposition on Pd results in C and H_2.[38−42]

The dimethyl disulfide molecules, $(CH_3S)_2$, in the gas phase act as a reservoir interchanging molecules with the surface at a given pressure and temperature. Defining the chemical potential of the MT with respect to the $(CH_3S)_2$ molecule as

$$\mu_{MT} = \frac{1}{2}[E_{(CH_3S)_2} + E^{ZPE}_{(CH_3S)_2}] + \Delta\mu \quad (4)$$

The total energy, $E_{(CH_3S)_2}$, and the zero-point energy, $E^{ZPE}_{(CH_3S)_2}$, of the dimethyl disulfide in the gas phase were computed by employing a cubic supercell with side lengths of $(20 \times 20 \times 20)$ Å^3. It should be pointed that $\Delta\mu$ contains the dependence with the experimental dimethyl disulfide pressure ($p_{(CH_3S)_2}$) and temperature (T), by the equation

$$\Delta\mu(T,p) = \frac{\mu^{\circ}_{(SCH_3)_2}(T,p^{\circ})}{2} + \frac{k_B T}{2}\ln\left(\frac{p_{(SCH_3)_2}}{p^{\circ}}\right) \quad (5)$$

where $\mu^{\circ}_{(SCH_3)_2}(T,p^{\circ})$ is the chemical potential relative to the standard pressure, p°, which has been estimated in terms of the molecular partition function as shown in the Supporting Information. To calculate the chemical potential of the hydrogen molecule, we have used eq 6

$$\mu_{H_2}(T,p) = E_{H_2} + E^{ZPE}_{H_2} + \mu^{0}_{H_2}(T,p^{0}) + k_B T \ln\left(\frac{p_{H_2}}{p^{0}}\right) \quad (6)$$

where k_B is the Boltzmann constant. The total energy E_{H_2} and the zero-point energy correction $E_{H_2}{}^{ZPE}$ were estimated by DFT, and $\mu_{H_2}{}^{0}$ can be taken from standard thermochemical tables.[30] We have used in our calculations $T = 300\ K$ and $p_{H_2} = 5 \times 10^{-7}$ atm. This value is reasonable, taking into account the H_2 levels in a recipient containing ethanol in contact with the atmosphere, typical for self-assembly from solutions. The chemical potential of carbon was fixed at $\mu_C = -11.8$ eV. This value can be determined by means of eqs 3−6 at the aforesaid $(CH_3S)_2$ and H_2 pressures and assuming for μ_S the value of the heat of formation of palladium sulfide, Pd_3S.[43] Note that, at this value, the Pd/C phase is not formed because it needs $\mu_C = -8.8$ eV to initiate carbon deposition.[44,45]

The definitions of the chemical potentials in eqs 4 and 5 permit one to write an expression for the surface free energy of the total system as a function of $\Delta\mu$ ($\gamma(\Delta\mu)$), which takes into account the amount of dimethyl disulfide in the gas phase as

$$\gamma(\Delta\mu) = \frac{1}{A}\left[E_{total} - N_{Pd}E^{bulk}_{Pd} + N_S\left(\mu_C + \frac{3}{2}\mu_{H_2}\right) - \frac{(N_S + N_{MT})}{2}[E_{(CH_3S)_2} + E^{ZPE}_{(CH_3S)_2}]\right] - \gamma_{clean} - \frac{(N_S + N_{MT})}{A}\Delta\mu \quad (7)$$

3. Preparation of the Alkanethiol SAMs on Pd and XPS Characterization

Palladium substrates were prepared by electrodeposition onto a preferred oriented Au(111) substrate prepared by annealing a polycrystalline Arrandee gold film evaporated on glass (see the Supporting Information for details). For the adsorption of 1-propanethiol (PT) on Pd, PT was used as received (Fluka, 99%) and the substrates were incubated in a 50 μM PT ethanolic solution overnight. After the incubation, the substrates were carefully rinsed with ethanol to eliminate unbound thiols. Details about XPS measurements are shown in the Supporting Information.

4. Results and Discussion

In the following, we describe the five models studied for the adsorption of methanethiol radical (MT) on Pd(111). Model 1 consists of a $(\sqrt{3} \times \sqrt{3})$R30° MT/Pd(111), with MT placed on the fcc hollow slightly shifted to the bridge site, which is the most stable position for this system (Figure 1a).[15] Model 2 corresponds to a $(\sqrt{3} \times \sqrt{3})$R30° S/Pd(111) lattice, where the S atom occupies a 3-fold fcc hollow site (Figure 1b).[24] Model 3 is a $(\sqrt{7} \times \sqrt{7})$R19.1° S structure reported by Liu et al.,[26] which was proposed to be the most stable between different S/Pd(111) surface structures (Figure 1c).[27] In this model the topmost layer of Pd(111) is formed by a mixed S−Pd structure (S_3Pd_5) with a packed arrangement of Pd pentagons with one S atom inside and two triangles with two S atoms. Model 4 has two MTs placed on top of the surface of model 3, $(\sqrt{7} \times \sqrt{7})$R19.1° S, with a 2/7 MT coverage. In this model the MT species are initially placed in a hollow-bridge position between two Pd atoms (see Figure S3 in the Supporting Information). This configuration reconstructs completely the S_3Pd_5 overlayer as a Pd atom becomes finally an adatom that binds two MT species (Figure 1d). This MT−Pd adatom−MT unit is similar to that proposed for thiols on gold.[6,7,46−48] In model 5 the atomic S atoms were incorporated into the bulk metal between the two topmost layers[28] with the same coverage as that found in models 3 and 4 (see Figure S4 in the Supporting Information). The subsurface S adsorption induces a noticeable structural distortion of the Pd(111) surface overall in the Pd topmost layer (Figure 1e). The MT species are adsorbed in a quasi bridge position and promote a strong reconstruction of the primitive Pd and S layers, giving rise to a S_3Pd_4 overlayer and three Pd adatoms. This model resembles the gold adatom-linked RS−Au−SR chains proposed for thiols on gold.[49]

The similarities and differences between models 4−5 and the Au adatom models described in refs 6, 7, and 49 are shown in Figures S5 and S6 of the Supporting Information. In model 4 each

(38) Shah, N.; Panjala, D.; Huffman, G. P. *Energy Fuels* **2001**, *15*, 1528–1534.
(39) Dropsch, H.; Baerns, M. *Appl. Catal. A: Gen.* **1997**, *165*, 159–169.
(40) Spiess, F.; Suib, S. L.; Irie, K.; Hayashi, Y.; Matsumoto, H. *Catal. Today* **2004**, *89*, 35–45.
(41) Takenaka, S.; Shigeta, Y.; Tanabe, E.; Otsuka, K. *J. Phys. Chem. B* **2004**, *108*, 7656–7664.
(42) Lin, Y.; Rei, M. *Int. J. Hydrogen Energy* **2000**, *25*, 211–219.
(43) Zubkov, A.; Fujino, T.; Sato, N.; Yamada, K. *J. Chem. Thermodyn.* **1998**, *30*, 571–581.
(44) Teschner, D.; Révay, Z.; Borsodi, J.; Hävecker, M.; Knop-Gericke, A.; Schlögl, R.; Milroy, D.; Jackson, S. D.; Torres, D.; Sautet, P. *Angew. Chem., Int. Ed.* **2008**, *47*, 9274–9278.
(45) Wrobel, R. J.; Becker, S. *Vacuum* **2010**, *84*, 1258–1265.
(46) Jiang, D.; Tiago, M. L.; Luo, W.; Dai, S. *J. Am. Chem. Soc.* **2008**, *130*, 2777–2779.
(47) Voznyy, O.; Dubowski, J. J. *Langmuir* **2009**, *25*, 7353–7358.
(48) Li, Y.; Galli, G.; Gygi, F. *ACS Nano* **2008**, *2*, 1896–1902.
(49) Jiang, D. *Chem. Phys. Lett.* **2009**, *477*, 90–94.

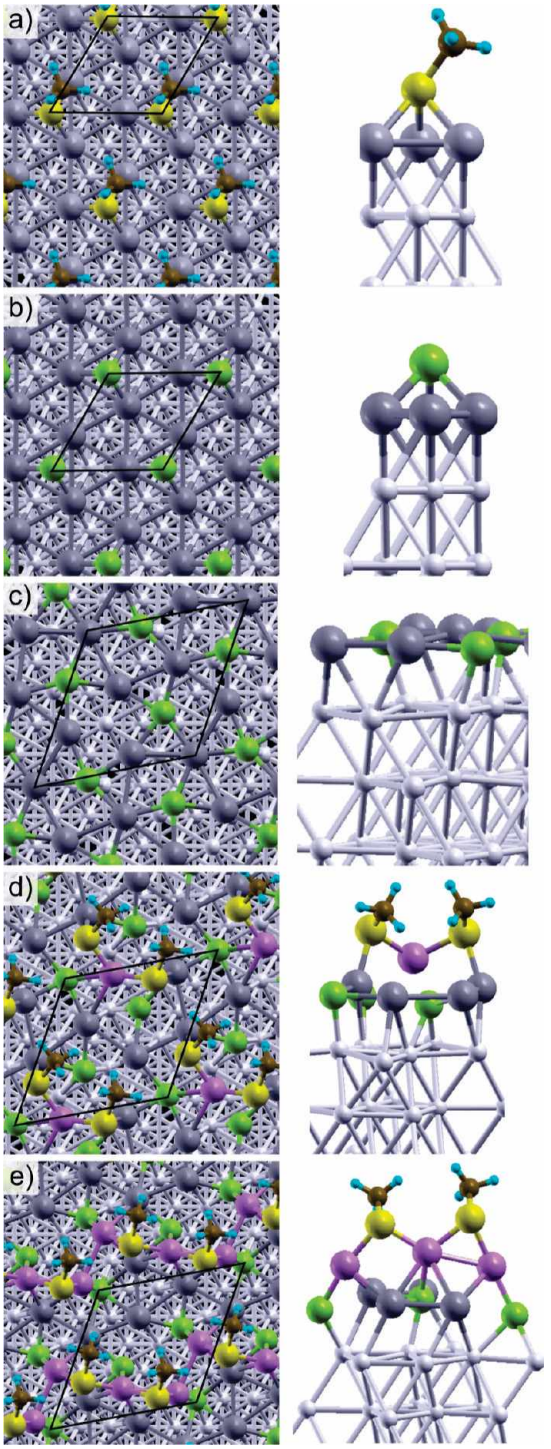

Figure 1. Different optimized surface models considered for MT/S adsorbed on Pd(111) surface: (a) model 1; (b) model 2; (c) model 3; (d) model 4; (e) model 5. S, green; S in MT, yellow; C, brown; H, cyan; Pd adatom, violet; Pd topmost layer, dark gray; Pd second and deeper layers, light gray.

S head of the adsorbed MT is bonded to a Pd adatom and also to a Pd surface atom at a quasi top position (Figure S5a), in a configuration very similar to that shown in the Au-adatom model described in refs 6 and 7 (Figure S5b). On the other hand, a chain structure between the metal adatoms and MT species (Figure S6a) can be observed for model 5, a structure resembling that described for MT on Au(111) in ref 49 (Figure S6b). However, unlike the Au adatom model, where two Au adatoms are bonded to two MT, in model 5 there are three Pd adatoms bonded to two MT. Note that two Pd of the three adatoms form a Pd−Pd bond with the same distance observed in bulk Pd (as in the case of the model described in ref 49 for MT on Au), whereas the third Pd adatom is closer to the Pd surface. This adatom would play the same role as the surface Au atom at which the MT is bonded at the top position.

In Table 1, the S and MT binding energies (E_b), S and MT coverages (θ), and structural parameters for the different surface models are shown. The E_b values for MT and S adsorbed on the Pd and S/Pd surfaces (models 4 and 5) were estimated from the equations

$$E_b^{MT} = \frac{1}{N_{MT}}(E_{total} - E_{Pd}(E_{Pd@S})_{4-5} - E_{MT}) \quad (8)$$

$$E_b^{S} = \frac{1}{N_S}(E_{total}(E_{Pd@S})_{4-5} - E_{Pd} - E_S) \quad (9)$$

where E_{MT}, E_S, E_{Pd}, and $E_{Pd@S}$ represent the total energies of the isolated radical MT, the S atom, and the relaxed bare Pd(111) or S/Pd(111) surfaces (models 4 and 5), respectively.

Results depicted in Table 1 show that the E_b values for S are twice that estimated for the adsorbed MT molecule on either bare or S-modified Pd(111). On the other hand, for the adsorbed MT E_b is greater than those estimated for MT adsorption on unreconstructed (E_b = −1.82 eV) and reconstructed Au(111) containing Au adatoms (E_b = −2.30/−2.50 eV).[41]

The surface free energy (γ) for the different surface structures on the Pd(111) substrate as a function of the chemical potential of MT, calculated with eq 7, is shown in Figure 2a. The surface free energy of the clean surface (γ_{clean}), estimated by eq 2, is also included. As expected, the surface free energy of the clean substrate surface is independent of the chemical potential of the MT; thus, it appears as a parallel line to the x-axis. On the other hand, the different S and/or MT surface structures on Pd(111) surface yield γ versus $\Delta\mu$ straight lines with different slopes, as shown in Figure 2. At low chemical potentials ($\Delta\mu \rightarrow -\infty$) the MT/S surface structures exhibit surface free energies values more positive than the γ_{clean}^{U}, reflecting that they are unstable with respect to the clean surface.

However, when $\Delta\mu$ = −5.40 eV, the ($\sqrt{3} \times \sqrt{3}$)R30° S lattice (model 2) becomes more stable than the clean Pd(111). Note that the ($\sqrt{3} \times \sqrt{3}$)R30° MT lattice (model **1**) would be more stable than the clean Pd(111) surface only when $\Delta\mu$ = −2.20 eV; that is, this surface structure should not be formed on Pd(111) because the ($\sqrt{3} \times \sqrt{3}$)R30° S lattice is thermodynamically favored. However, the S−C bond cleavage is not a low-energy process, which suggests that the ($\sqrt{3} \times \sqrt{3}$)R30° thiol lattice could exist as a kinetically stabilized system, but at present there is no experimental evidence for the formation of a sulfide-free ($\sqrt{3} \times \sqrt{3}$)R30° alkanethiolate structures on Pd(111). The formation of the ($\sqrt{3} \times \sqrt{3}$)R30° S lattice implies that, under these conditions, adsorbed MT species have broken their S−C bonds, giving rise to adsorbed S species. The chemical potential range for the thermodynamic stability of the ($\sqrt{3} \times \sqrt{3}$)R30° S surface structure extends to $\Delta\mu$ = −4.60 eV, where it undergoes a transition forming the ($\sqrt{7} \times \sqrt{7}$)R19.1° S (model 3) surface structure. This surface structure is stable up to $\Delta\mu$ = −1.2 eV, where the ($\sqrt{7} \times \sqrt{7}$)R19.1° (S + MT) lattices "on surface" (model 4) or at "subsurface" (model 5) start to dominate the phase diagram. This means that MT adlayers on Pd become stable only when the Pd surface is largely passivated with S atoms. The difference in stability between the "on surface" (model 4) and "subsurface"

Table 1. Different Models (1−5) for the MT/S Surface Structures on Pd(111)[a]

					E_b/eV		S	MT		
model	lattice	θ_{Pd}	θ_{MT}	θ_S	S	MT	d_{Pd-S}/Å	d_{Pd-S}/Å	d_{S-C}/Å	α/deg
1	$(\sqrt{3} \times \sqrt{3})$R30° MT	0	1/3	0		−2.67		2.35	1.86	37
2	$(\sqrt{3} \times \sqrt{3})$R30° S	0	0	1/3	−4.98		2.25			
3	$(\sqrt{7} \times \sqrt{7})$R19.1° S	5/7	0	3/7	−5.50		2.36			
4	$(\sqrt{7} \times \sqrt{7})$R19.1° (S + MT)	5/7	2/7	3/7	−5.70	−2.62	2.47	2.38	1.82	54
5	$(\sqrt{7} \times \sqrt{7})$R19.1° ($S_{sub}$+MT)	7/7	2/7	3/7	−5.58	−3.22	2.45	2.33	1.83	58

[a] Metal and adsorbate coverage (θ_{Pd}, topmost layer), θ_{MT}, and θ_S) are indicated. DFT predicted parameters interatomic average distance (d_{Pd-S}, d_{S-C}), tilt angle (α, the angle between the S−C bond and the surface normal), and binding energies (E_b) of the adsorbates (eqs 8−9) are shown.

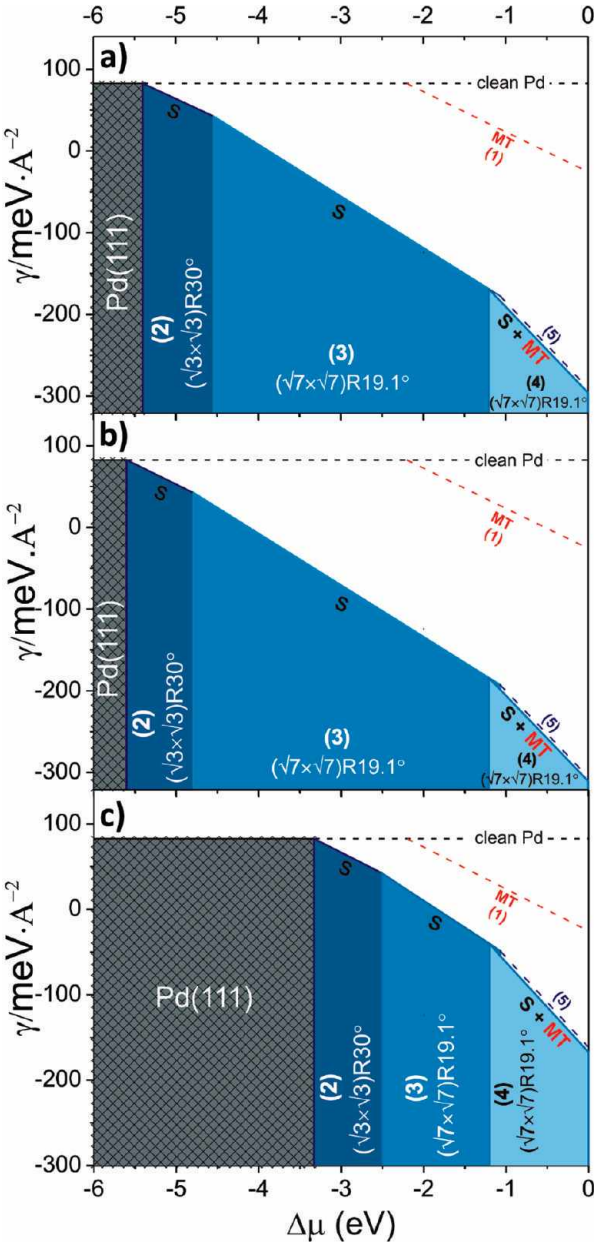

Figure 2. Surface free energy (γ) of different surface structures on Pd(111) as a function of the chemical potential of the MT: (a) T = 300 K, $p_{H_2} = 5 \times 10^{-7}$, atm $\mu_C = -11.8$ eV; (b) T = 300 K, $p_{H_2} = 1 \times 10^{-9}$ atm, $\mu_C = -11.8$ eV; (c) T = 300 K, $p_{H_2} = 5 \times 10^{-7}$ atm, $\mu_C = -9$ eV. Dashed lines: red, $(\sqrt{3} \times \sqrt{3})$R30° MT (model 1); blue, $(\sqrt{7} \times \sqrt{7})$R19.1° (S + MT) at "subsurface" (model 5). The difference in γ between the $(\sqrt{7} \times \sqrt{7})$R19.1° (S + MT) "on surface" (model 4) and "at subsurface" (model 5) is 5.6 meV. The numbers in the figure indicate the model.

(model 5) structures is 5.6 meV/Å^2. This energy difference is of the order of the thermal energy; therefore, any of these structures would be expected. It is worth nothing that the simultaneous adsorption of S and MT molecules strongly reconstructs the Pd surface (Figure 1d,e).

It should be noted that the $\theta_{sulfide} \approx 0.4$ and $\theta_{thiolate} \approx 0.3$ could be also consistent with a $(\sqrt{3} \times \sqrt{3})$R30° S overlayer + $(\sqrt{3} \times \sqrt{3})$R30° thiol lattice ($\theta_S = 0.66$). However, the DFT calculations and thermodynamic analysis indicate that this surface structure is much more unstable than those corresponding to models 4 and 5. In fact, the γ versus $\Delta\mu$ plot for this lattice runs practically parallel to the lines of models 4 and 5 (Figure 2a) but shifted approximately 50 meV/Å^2 to more positive values. Finally, we have observed that a noticeable change in p_{H_2} from 5×10^{-7} to 10^{-9} atm results in only small changes in the stability diagram (Figure 2b). On the other hand, the increase in μ_C from −11.8 eV (Figure 2a) to −9.0 eV (Figure 2c), a value close to the value at which C starts to be incorporated into Pd,[44] hinders the formation of the S phases but has no effect on the $(\sqrt{7} \times \sqrt{7})$R19.1° (S + MT) stability region.

We have seen in the analysis of the stability diagram (Figure 2) how strong is the reactivity of the Pd(111) surface against the MT adsorption. To gain more insight into the MT/Pd interaction, we provide in Figure 3, the electronic description of the evolution on the thiol adsorption on Pd(111) in light of the calculated projected density of states (PDOS). According to the *d*-band theory relative to the reactivity of transition metals, to make and break adsorbate bonds, the closer the *d*-band center is to the Fermi level, the easier the charge transfer between the metal surface and the adsorbate states. In Figure 3a,b the PDOS analysis for the MT radical and the clean Pd(111) surface are shown. Figure 3c (model 1) shows how the MT−Pd interaction reduces the Pd *d*-DOS near the Fermi level compared with Pd atoms in the clean surface and how this *d*-band is broadened. The bonding molecular orbitals of MT are stabilized because their energy levels are decreased and broadened with respect to the isolated molecule (Figure 3b). The antibonding MT molecular orbitals (mainly of π character), which in the gas phase (Figure 3a) are at the Fermi level, are now hybridized with the Pd *d*-band and, therefore, they are more delocalized. Electron transfer from the metal *d*-band to the antibonding orbitals weakens the S−C bond. This fact results in the elongation of the S−C bond length (d_{S-C} = 1.86 Å) with respect to the MT radical in vacuum (d_{S-C} = 1.79 Å) and also the accumulation of negative charge in the C atom after thiol adsorption (see Tables 1 and 2). In Figure 3d,e (corresponding to models 2 and 3) it is clear how the S atoms work via modification of the electronic structure of Pd(111) substrate. One can observe the strong overlap between the S(*s*,*p*) and the *d*-band that shifts toward more negative values, inducing a large reduction in the *d* states near the Fermi level (Table 2). Finally, the PDOS diagrams for models 4 and 5 (Figure 3f,g) also show that the position of the center of the metal *d*-band (ε_d) involved in the

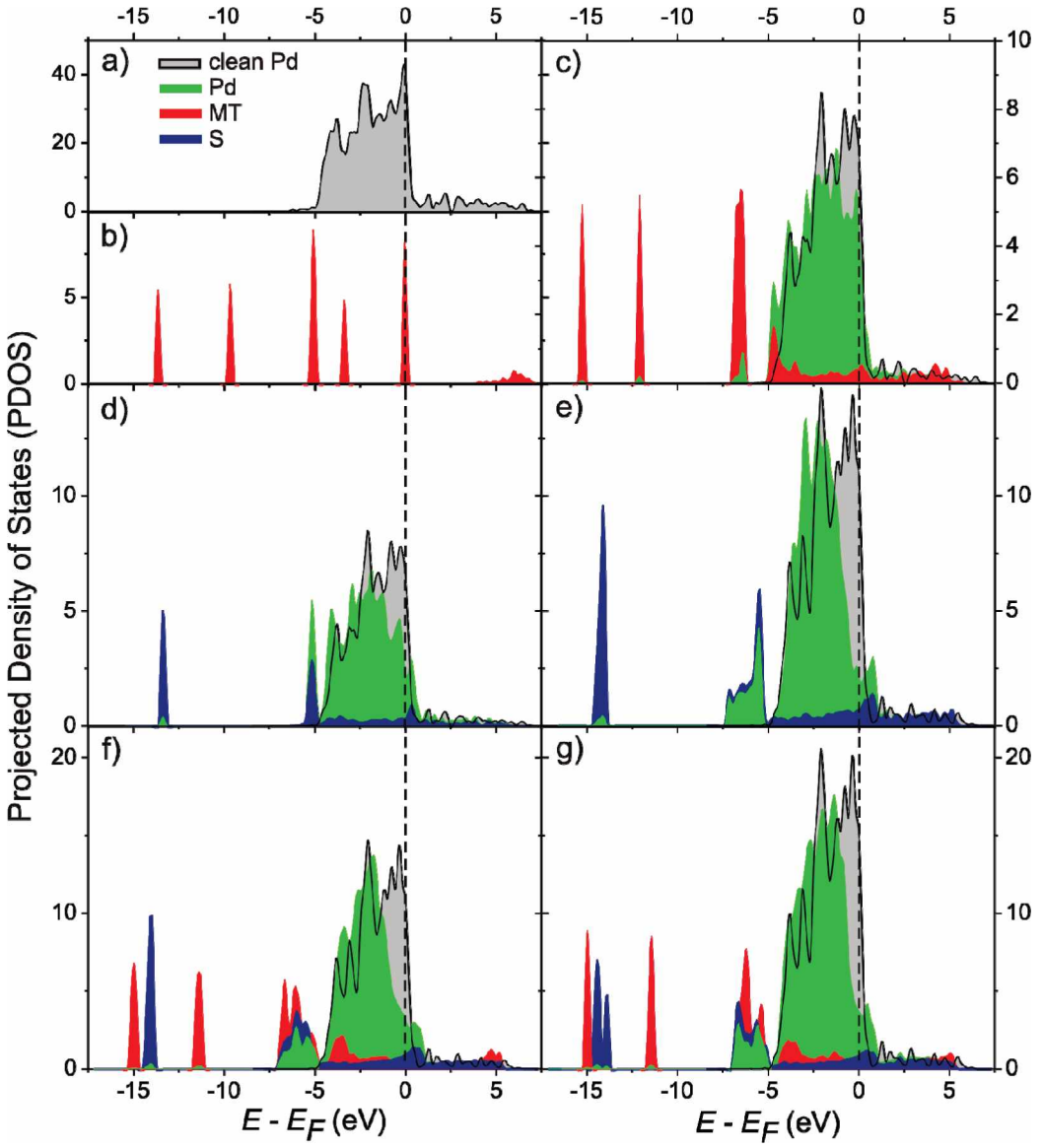

Figure 3. Projected density of states (PDOS) (E_{Fermi} (E_F) = 0 eV) of the different systems studied: (a) clean Pd(111); (b) isolated MT; (c) model 1; (d) model 2; (e) model 3; (f) model 4; (g) model 5. Gray, clean Pd (top atoms), d states; green, Pd (top atoms), d states; red, MT, s and p states; blue, S, s and p states.

Table 2. Energy of the Center of the Metal *d*-Band with Respect to the Fermi Energy (ε_d) and Bader Charges Calculated for the Different Models

		Bader charges/e			
			MT		
model	ε_d/eV	top Pd layer atoms	S	C	S
1	−1.75	+0.06	−0.20	−0.03	
2	−1.85	+0.09			−0.22
3	−1.83	+0.21			−0.42
4	−1.83	+0.36 (adatom)	−0.16	−0.06	−0.39
		+0.21			
5	−1.83	+0.44 (adatom)	−0.17	−0.10	−0.40
		+0.14		−0.04	

PdS structures lowers its value with respect to the Fermi level (Table 2). Therefore, these overlayers are not so active for the dissociation of MT in relation to the clean Pd(111) surface. In fact, the PdS surface becomes less reactive; hence, it cannot break the S−C bond and, accordingly, the MT adsorption becomes possible.

The center of the metal *d*-band (ε_d) position for the different models is summarized in Table 2. The shift in ε_d with respect the clean Pd(111) surface (ε_d = −1.69 eV) after S adsorption is evident, thus explaining the "passivation" of the surface that finally allows MT adsorption with no S−C bond cleavage. A shift in ε_d was experimentally observed by photoelectron spectroscopy of the valence band, in alkanethiol-protected Pd nanoparticles.[50] This passivation is evident, because the PDOS of the S/Pd is similar to that of the Au(111) surface (see Figure S7 in the Supporting Information), where it is well established that no S−C cleavage occurs; that is, no further sulfidization should take place. We have also made the Bader analysis to obtain quantitative information about the charge transfer induced by MT adsorption (Table 2). Positive values indicate charge gain, whereas negatives values indicate the opposite process. Particularly, we focus on the top Pd atom layer and on the S and C atoms. Results in Table 2 clearly show that S adsorption induces a marked charge transfer from the Pd surface to the S atom.

(50) Cook, S. C.; Padmos, J. D.; Zhang, P. *J. Chem. Phys.* **2008**, *128*, 154705–11.

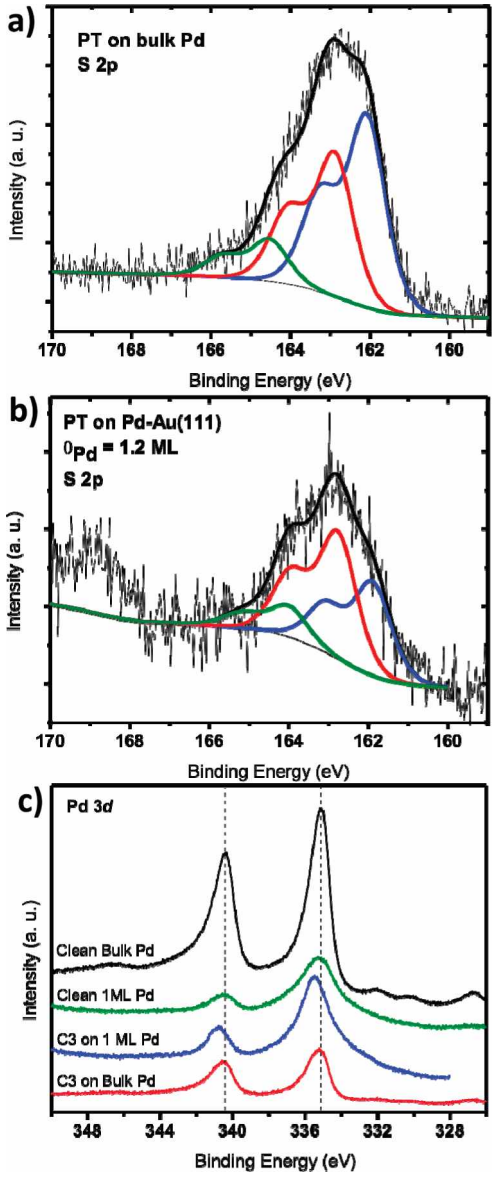

Figure 4. S 2p and Pd 3d signals of the XPS spectra of different PT-modified and clean Pd surfaces: (a) S 2p signal of PT-modified bulk Pd; (b) S 2p signal of PT-modified 1.2 ML Pd−Au(111); (c) Pd 3d signal of the XPS spectra of clean and PT-modified Pd surfaces. Dashed lines correspond to the binding energies of the Pd $3d_{3/2}$ and Pd $3d_{5/2}$ signals of clean Pd. In the case of Pd−Au(111), the Pd $3d_{5/2}$ signal has also a contribution from the Au $4d_{5/2}$ signal.

In the following, XPS measurements are shown, and the results are compared with the theoretical calculations. Figure 4a shows a typical XPS S 2p spectrum obtained after immersion of a (111) preferred oriented Pd sample in a 50 μM propanethiol (PT) ethanolic solution overnight.

We interpret the three components needed to fit the S 2p spectrum shown in Figure 4a following refs 3 and 23. The 162.9 and 162.1 eV components were assigned to thiolate SAM and to a diluted sulfide layer, respectively. On the other hand, the assignment of the small 164.1 eV component can be related to S_n species.[3]

To study the effect of the Pd layers below the top layer on thiol adsorption, a substrate with nearly one Pd monolayer (1.2 ML) was prepared on a preferred oriented Au(111) substrate by underpotential deposition (UPD) (see the Supporting Information). Afterward, the adsorption of PT on it was performed in the same way as with bulk Pd. XPS data for S 2p signal

Table 3. Relative Contribution of the Different Components of the S 2p Signal for PT on Bulk Pd and 1.2 Pd Monolayers (ML) and the Ones Calculated for Models 4 and 5[a]

	Pd Bulk	1.2 ML Pd−Au(111)	models 4 and 5
sulfide	48%, 0.4 ML	13%, 0.15 ML	3/7 = 0.43 ML
thiolate	39%, 0.3 ML	18%, 0.22 ML	2/7 = 0.29 ML
S + T	0.7 ML	0.37 ML	5/7 = 0.71 ML

[a] S + T is the sum of the coverage of sulfide and thiolate. The percentages are calculated by taking into account all of the sulfur species present.

(Figure 4b) also show three components at nearly the same binding energies as in bulk Pd with relative quantities shown in Table 3. The peak at higher binding energy is assigned to some sulfates, which could come from the electrodeposition electrolyte. It is worth nothing that in this case the relative amount of the sulfide component strongly decreased with respect to bulk Pd. This means that only 0.15 S ML was necessary to allow the PT adlayer to be adsorbed on the surface without S−C bond scission, in contrast to the 0.4 S ML observed on bulk Pd. This result is evidence that the Pd atomic layers below the top layer might play a crucial role in the formation of the $(\sqrt{7} \times \sqrt{7})$R19.1° S layer. In both models 4 and 5, the second Pd atomic layer bonds to S atoms (Figure 1d,e). Therefore, the two models are supported by XPS data of bulk Pd and 1.2 Pd ML.

The Pd 3d spectra for these systems are shown in Figure 4c. A clear positive binding energy shift of the Pd 3d signal is observed for the thiol-covered Pd surfaces, a fact that is more evident for the sample of 1.2 Pd ML. We interpret these results in terms of the calculated Bader charges shown in Table 2. In fact, +0.36 and +0.44 charges on Pd are observed for models 4 and 5, respectively. These charges are higher than those observed for unreconstructed (+0.04) or adatom reconstructed Au (+0.12/+0.15) models when thiols are adsorbed on these substrates. This little charge on Au explains the fact that no binding energy shift is observed on Au 4f XPS signals:[51] the contribution of surface Au atoms with this charge to the Au 4f signal is negligible when compared with the contribution of zero charge from deeper Au layers. In Pd, however, the charge is high enough to produce a shift to higher binding energy in the Pd 3d signal, even when bulk Pd is used. It is worth noting that, as expected, the major contribution to the positive charge on Pd comes from the presence of the $(\sqrt{7} \times \sqrt{7})$R19.1° S layer (see Table 2) of the proposed models. Moreover, it has been reported that adsorption and dissociation of S_2 on Pd(111) and polycrystalline Pd, leading to the formation of Pd−S bonds, induce large positive binding energy shifts in the core and valence levels of Pd.[52]

5. General Discussion

Data in Table 3 also show the close correlation between the thiol coverages from XPS data for bulk Pd and the ones calculated for models 4 and 5. The pressure of the thiol in the gas phase for each chemical potential can be calculated with eq 5. The extremely low transition pressure of $\sim 10^{-27}$ atm or thiol concentration of $\sim 10^{-32}$ M (see the Supporting Information) between the $(\sqrt{7} \times \sqrt{7})$R19.1° S structure (model 3) and the $(\sqrt{7} \times \sqrt{7})$R19.1° (S + MT) lattices (models 4 and 5) shows that the sulfide layers without adsorbed MT are not, in a first approximation, experimentally achievable. Hence, the experimentally accessible surface structure for thiols adsorbed on Pd, under thermodynamic equilibrium,

(51) Vericat, C.; Vela, M. E.; Benitez, G.; Carro, P.; Salvarezza, R. C. *Chem. Soc. Rev.* **2010**, *39*, 1805–1834.
(52) Rodriguez, J. A.; Chaturvedi, S.; Jirsak, T. *Chem. Phys. Lett.* **1998**, *296*, 421–428.

should be the one that comprises the thiolates adsorbed onto the sulfide layer. This means that the other surface structures would be observed only if they were kinetically trapped. It could be possible to think that S can diffuse inside bulk Pd, leaving a clean Pd surface capable of breaking the S−C bonds of the adsorbed thiols and leading to a sulfidized surface without hydrocarbon moieties. However, it should be noted that S diffusion into Pd was observed only when the sulfide surface coverage was >0.75 ML,[28] which is much larger than the 0.4 ML experimentally observed for the sulfide layer in models 4 and 5. On the other hand, the oxidation of the thiol/S adlayer has been described, but only when the system is exposed to atmospheric oxygen for some days.[3]

Note that some amount of S−S species is present in the experimental sample (Table 3) when the total amount of sulfur is close to 0.7 as already predicted.[28] This contribution was not included in our models. It can also be argued that a comparison between MT and PT is not valid because dispersive forces should enhance the stability of the different thiol surface structures. However, for short thiols such as PT, the contributions of dispersive forces are expected to be weak ($\approx$0.04 eV per C atom).

With regard to the calculated binding energies of thiol and sulfides (E_b) (Table 1), they can be related with the electrodesorption potentials of thiols on metals, which are studied electrochemically. As a first approach, as the E_b is higher, the electrodesorption potential of thiols is more negative. It can be observed in Table 2 that the E_b of MT in model 4 ($E_b = -2.62$ eV) is higher than the one of MT on unreconstructed ($E_b = -1.80$ eV) or even on reconstructed ($E_b = -2.34/-2.48$ eV) Au(111).[51] These results are in concordance with our previous electrodesorption experiments. In fact, we have observed that alkanethiols adsorbed on Pd show an increased stability toward electrochemical desorption compared with alkanethiols on Au.[23]

Finally, we propose the following scenario for the adsorption of thiols on Pd(111) surfaces. After adsorption of thiols, the S−C bond is enlarged and cleaved because the diluted sulfide surface structure is energetically more stable than a similar thiolate adlayer on Pd. This different behavior from the adsorption of thiols on Au should be understood considering the differences in the electronic structure between both metals, mainly focused in the center of the *d*-band and the degree of filling of the *d*-band. The system incorporates more sulfur up to a level at which the energy barrier for S−C bond cleavage becomes too high and, therefore, the thiol molecules can be coadsorbed on the S-terminated Pd surface. This is supported by the fact that predicted H_2 dissociation barriers are higher on the S-terminated Pd_4S surfaces than on clean Pd surfaces.[53]

(53) Miller, J. B.; Alfonso, D. R.; Howard, B. H.; O'Brien, C. P.; Morreale, B. D. *J. Phys. Chem. C* **2009**, *113*, 18800–18806.

6. Conclusions

We have shown, by means of DFT calculations, the reasons for the presence of the sulfide layer in the adsorption of alkanethiols on Pd(111). Different surface structures are formed on Pd when the chemical potential of the thiol is changed, as shown from first-principles atomistic thermodynamics computations. This information is important to understand the complex chemical reactions that take place between thiol molecules and palladium surfaces. The two more stable lattices found (models 4 and 5), with sulfide either "on surface" or "subsurface", are both feasible to be the ones experimentally observed, although other more stable structures could also be possible. Interestingly, the thiols on these systems are arranged in structures similar to some of the ones proposed for thiols on Au(111).

Acknowledgment. We acknowledge financial support from ANPCyT (Argentina, PICT06-621, PICT05-32980), CONICET (Argentina, PIP 112-200801-362), and MCI (Spain, CTQ2008-06017/BQU). G.C. acknowledges a doctoral fellowship provided by CONICET.

Supporting Information Available: Details of the computational methods, the derivation of the thermodynamic equations, the calculation of the standard chemical potential of dimethyl disulfide, the structural properties of models studied, and the experimental aspects related to the preparation of palladium substrates as well as the XPS characterization. This material is available free of charge via the Internet at http://pubs.acs.org.